# Elasticity of (K,Na)AlSi3O8 hollandite from lattice dynamics calculations

R. Caracas, T. Boffa Ballaran

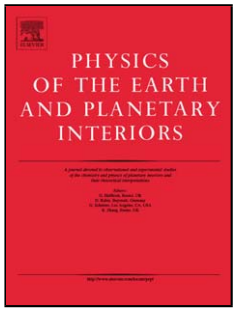


Title: Elasticity of (K,Na)AlSi3O8 hollandite from lattice dynamics calculations

Authors: R. Caracas, T. Boffa Ballaran

PII: S0031-9201(10)00072-5
DOI: doi:10.1016/j.pepi.2010.04.004
Reference: PEPI 5277

To appear in: *Physics of the Earth and Planetary Interiors*

Received date: 9-11-2009
Revised date: 17-3-2010
Accepted date: 10-4-2010

Please cite this article as: Caracas, R., Ballaran, T.B., Elasticity of (K,Na)AlSi3O8 hollandite from lattice dynamics calculations, *Physics of the Earth and Planetary Interiors* (2008), doi:10.1016/j.pepi.2010.04.004

# Elasticity of (K,Na)$AlSi_3O_8$ hollandite from lattice dynamics calculations

R. Caracas[1] and T. Boffa Ballaran[2]

[1] *CNRS, Ecole Normale Supérieure de Lyon, Laboratoire de Sciences de la Terre UMR 5570, 46, allée d'Italie, 69364 Lyon cedex 07, France, e-mail: razvan.caracas@ens-lyon.fr*

[2] *Bayerisches Geoinstitut, Universität Bayreuth, Universitätstrasse 30, D-95440 Bayreuth, Germany*

**Abstract**

We compute the elastic constants tensor and the seismic properties of $KAlSi_3O_8$ and $K_{0.8}Na_{0.2}AlSi_3O_8$ up to the ferroelastic transition using density-functional theory and density-functional perturbation theory in the ABINIT implementation. We observe a softening of the tetragonal shear with pressure that precedes the ferroelastic transition. The Reuss shear moduli become negative at respectively 23 GPa and 13 GPa for the two compositions considered in here. The ferroelastic transition is associated with a strong decrease of the horizontal shear wave velocities and a corresponding increase of the seismic anisotropy. The presence of Na enhances these features.

## 1 Introduction

The large alkaline and calc-alkaline cations like K, Na, Ba, Sr are usually incompatible with the silicatic mantle and thus they tend to fractionate in the Earth's crust. They can get entrained by the subduction and penetrate in the mantle. In this geological setting their major transport means are open-framework structures, like feldspars, certain micas and amphibole, and especially the mineral hollandite (Downs et al., 1995). At low and moderate thermodynamic conditions prevalent in the beginning and the early stages of the subduction process the main mineral hosts for K in the subducting slabs are the phengite micas, the feldspar, the wadeite and the amphiboles (Irifune et al., 1994, Dobrzhinetskaya and Green, 2007, Konzett and Fei, 2000). The stability field of hollandite within the thermochemical conditions of the upper mantle is reached at about 8-9 GPa, corresponding to depths of about 300 km (Irifune et al., 1994, Urakawa et al., 1994, Schmidt, 1996, Tutti et

al., 2001, Akaogi et al., 2004, Yong et al., 2006, Dobrzhinetskaya and Green, 2007). Once formed the hollandite can stay within this form up to very high pressures and could potentially be transported even into the lower mantle (Hirao et al., 2008). The ferroelastic phase transition, characterized by a positive Clapeyron slope, appears at depths of about 400 to 500 km depending on the composition. Afterwards hollandite is stable throughout the Earth's mantle. The two structures, hollandite I, tetragonal, stable before the transition and hollandite II, monoclinic, stable after the transition are very similar. In the following we study the low-pressure polymorph, hollandite I that we will denote hereinafter simply as hollandite.

The crystal structure of hollandite (Fig. 1) consists of tunnels with a square cross-section, which run parallel to the fourfold axis. The tunnels are delimited by double chains of edge-sharing octahedra. The cations inside the tunnels are usually monovalent or divalent and the cations inside the octahedra are trivalent or tetravalent. The possible size mismatch between the cations inside the tunnels and the cations inside the octahedra may induce crystallographic distortions leading to ferroelastic transitions under pressure or apparition in incommensurate structures at low temperatures (Caracas, 2002, Wu et al., 1991). From the geoscientific point of view the wide tunnels are an ideal host for geochemically incompatible elements, like K, Na, Ba and Sr or other large non-alkaline elements, like Pb and U. However, within the Earth's geochemical setting the major cation is K, which can be partially replaced by Na. Experiments suggest maximum sodium limit of about 40-50 at.% for characteristic upper mantle thermodynamics conditions (Yagi et al., 1994, Liu, 2006).

Recent in situ high-pressure studies of $KAlSi_3O_8$ hollandite (Sueda et al. 2004; Nishiyama et al. 2005; Ferroir et al. 2006; Hirao et al. 2008) reported a non-quenchable phase transformation from tetragonal to monoclinic symmetry at about 20 GPa. The high-pressure phase can be indexed with a monoclinic unit cell (space group I2/m) similar in structure with $BaMn_8O_{16}$ hollandite. The transition is described by the group-subgroup relation 4/m to 2/m for which the active representation is $B_g$ of the point group 4/m.

Here we consider two cases: pure $KAlSi_3O_8$ and 80 at. %K - 20 at. % Na, as $K_{0.8}Na_{0.2}AlSi_3O_8$, which are largely within the range of expected natural compositions from the Earth's upper mantle. We assume ideally disordered structures at all pressures with Si and Al randomly distributed inside the octahedra and K and Na randomly distributed on the K site, inside the tetragonal tunnels. All calculations are performed in the primitive unit cell of the conventional tetragonal I4/m one, which hosts one formula unit.

## 2 Computational details

We compute the full elastic constants tensor in the framework of the density functional perturbation theory (DFPT) (Baroni et al., 1987, Gonze et al., 1992, Gonze, 1997, Gonze and Lee, 1997, Baroni et al., 2001, Gonze et al., 2005a). Here the elastic constants are expressed as the derivative of the energy with respect to lattice strains (Hamman et al. 2005). The atomic relaxations due to strain are taken into account from the phonon and dielectric calculations by inverting a matrix containing the interatomic force constants, the couplings with the strains and the couplings with the electric fields. The elastic theory is implemented on top of the density functional theory (DFT) (Hohenberg and Kohn, 1964, Kohn and Sham, 1965) in the ABINIT package (Gonze et al., 2002, Gonze et al., 2005) based on planewaves and pseudopotentials.

We use the local density approximation for the exchange-correlation energy, with Troullier-Martins type pseudopotentials. As usual with planewave basis sets, the numerical accuracy of the calculation can be systematically improved by increasing the cut-off kinetic energy of the planewaves and the density of the sampling of the Brillouin zone (Payne et al., 1992). We use a 35 Ha cut-off energy for the kinetic energy of the planewaves. We sample the reciprocal space using a 8x8x8 regular grid of special k points according to the Monkhorst-Pack scheme (Monkhorst and Pack 1976).

The classical method to study an intermediate term of a solid solution is the cluster expansion model. According to this approach the properties of the disordered solid may be inferred using the computed results for only several selected supercells with different representative atomic configurations and then making use of statistical physics. This model is straightforward and it can be applied to any type of disordered structure or solid solution, but the results are highly dependent on the quality of the sampling. Each individual calculation is more tedious because of larger system sizes and possible losses of symmetry due to the specific atomic configuration.

Here we adopt an alternative approach, the virtual crystal approximation (Bellaiche and Vanderbilt, 2000). For each of the disordered sites we construct a new pseudopotential called *alchemical*, which is obtained from mixing the atoms that participate in the solid solution in the appropriate amounts (Giantomassi et al, 2005,). In practice the *alchemical* pseudopotentials are obtained as follows: the local potentials of the original pseudopotentials are linearly mixed, the form factors of the non-local projectors are all preserved, and all considered to generate the alchemical potential, the scalar coefficients of the non-local projectors are multiplied proportionally and the core charge cutoff radius and functions are linear combinations of respectively the radii and the functions of the original pseudopotentials.

This approach uses small simulation cells and preserves the symmetry, but the mixing should be realized between chemically similar atoms. It is especially well suited for solid solutions that do not show ordering on any scale. The theoretical structures and their physical properties obtained using the alchemical pseudopotentials are in very good agreement to experimental data. This latter approach has already been successfully applied to compute physical properties for solid solutions, like dielectric tensors (Cohen, 2007) or Raman and elasticity (Caracas and Banigan, 2009). For example, in spinel, $MgAl_2O_4$, it has been shown that only a partial Mg-Al disordering can explain the experimental results, as the purely ordered structure would yield Raman signatures whose intensities and artificial peak splitting disagree with the experiments. For hollandite there is no indication about ordering on any scale of neither K/Na nor Si/Al. Consequently the alchemical approach should give more reliable results than the use of supercells, no matter how complex they can be (Mookherjee and Steinle-Neumann, 2009).

## 3 Results and discussion

Hollandite is tetragonal with space group I4/m and two formula units in the conventional unit cell. The large cations, i.e. K, Na, etc., lay on the 2a Wyckhoff positions; the octahedrally coordinated cations, ı.e. Si and Al, are disordered on the 8h Wyckoff positions; the O atoms lay on 8h Wyckhoff positions. We perform the first-principles calculations using the primitive unit cell in order to avoid the phase-corrections of the wavefunctions (that would otherwise contribute from the neighboring Brillouin zone by folding back to the original zone). This same restriction is highly useful as it minimizes the computational effort by reducing the size of the unit cell. We chose the axis orientation such as the four-fold tunnel parallel to the c axis of the primitive unit cell.

The variation of the lattice parameters with pressure for the two compositions is summarized in Table 1. The Na-bearing hollandite has consistently smaller lattice parameters than the K-pure term. The change in density between the two compositions is almost entirely due to the difference in cationic masses. The internal atomic coordinates that are not fixed by symmetry are weakly affected by compression, as seen in Table 2. This is due to a bulk compression of the structure under pressure, as the tetragonal symmetry does not allow the octahedra forming the tetragonal tunnels to rotate one with respect to the other. Our theoretical structural data are in excellent agreement with the experimental data (Boffa Ballaran et al., 2009) with underestimations of the lattice parameters on the order of 1.5 %.

Hollandite belongs to the tetragonal Laue group TII, which contains all crystals with $\bar{4}$, $4/m$ and $\bar{4}/m$ point groups. For this class of symmetry there are

seven independent second-order elastic constants, which after full symmetrization of the elastic constants tensor are: $C_{11}$, $C_{12}$, $C_{13}$, $C_{33}$, $C_{44}$, $C_{66}$ and $C_{16}$.

The values of the elastic constants as a function of pressure are listed in Table 3. $C_{11}$ becomes smaller for the Na-bearing samples with increasing pressure. The difference between the K-pure term and the Na-bearing compositions is accentuated under pressure. $C_{12}$ and $C_{66}$ show a decrease between the K-pure and Na-bearing compositions. The decrease, roughly independent of pressure, is related to the change in size of the cations situated inside the tetragonal tunnels of the structure: the $K_{0.8}Na_{0.2}$ cation is smaller than pure K. This size difference also leads to a decrease of the unit cell volume by 0.7% at 20GPa, as discussed above. The effect on elastic constants is more important for $C_{66}$ (about 15% decrease) than $C_{12}$ (about 7% decrease). As a direct result the softening of the tetragonal shear, $C_{11}$-$C_{12}$, is different between K-pure and Na-bearing compositions, being more accentuated in the latter. $C_{44}$, $C_{13}$ and $C_{16}$ are weakly affected by the presence of Na, as they correspond to distortions of the $SiO_6$ octahedral framework of the structure.

The expression of the elastic moduli for crystals in the Laue TII symmetry class has not been derived analytically. The difficulty arises from the presence of the off-diagonal shear elastic constant $C_{16}$. However it is possible to define a rotation of the elastic constants tensor around the [001] axis with an angle $\theta$:

$$R(\theta) = \begin{vmatrix} cos(\theta) & -sin(\theta) & 0 \\ sin(\theta) & cos(\theta) & 0 \\ 0 & 0 & 1 \end{vmatrix} \quad (1)$$

in such a way that the resulting elastic constant $C'_{16}$ of the rotated tensor is zero. Using the full tensorial notation and the relation for tensor rotation:

$$C'_{ijkl} = \sum_{a,b,c,d} R_{ia} R_{jb} R_{kc} R_{ld} C_{abcd} \quad (2)$$

after solving out the math, the condition $\theta$ should fulfill is:

$$\theta = \frac{1}{4} atan(-\frac{4C_{1112}}{C_{1111} - C_{1122} - 2C_{1212}}) \quad (3)$$

.

In this new setting the number of symmetry-independent elastic constants is reduced to six: $C_{11}$, $C_{12}$, $C_{13}$, $C_{33}$, $C_{44}$ and $C_{66}$. Their variation with pressure is

shown in Figure 2. This procedure has been also described when characterizing the elasticity of selected scheelites (Farley et al., 1975, Blanchfield et al., 1982).

Standard formulas for the shear (G), bulk (K), and Young (Y) elastic moduli for the tetragonal Laue class I in the Voigt and Reuss averages, labeled with respectively subscripts V and R, can then be applied:

$$K_V = \frac{2C_{11} + C_{33} + 2C_{12} + 4C_{13}}{9} \tag{4}$$

$$G_V = \frac{2C_{11} + C_{33} - C_{12} - 2C_{13} + 6C_{44} + 3C_{66}}{15} \tag{5}$$

$$K_R = \frac{1}{2S_{11} + S_{33} + 2S_{12} + 4S_{13}} \tag{6}$$

$$G_R = \frac{15}{8S_{11} + 4S_{33} - 4S_{12} - 8S_{13} + 6S_{44} + 3S_{66}} \tag{7}$$

$$Y = \frac{9KG}{3K + G} \tag{8}$$

The Voigt elastic moduli of the two compositions are listed in Table 4 and their variation as a function of pressure is shown in Fig. 3. They show an almost linear increase with increasing pressure. The Na-bearing composition is softer than the K-pure term. The difference between the two compositions is accentuated with pressure, at about 1.8% at ambient pressure conditions and reaching about 7% reduction at 20GPa. The derivative of the elastic moduli versus pressure are respectively 1.20, 4.37 and 3.51 for the shear (G), bulk (K), and Young (Y) moduli in the K-end member and 0.55, 2.88 and 1.84 for respectively G, K and Y of the Na-bearing term. The bulk modulus in the Reuss formulation is positive, increases with pressure, and has a smaller but similar value as the one obtained from the Voigt average. The Poisson ratio, $\mu = Y/2G - 1$, has values between 0.23 up to 0.3, which follow in the normal range of values expected for ceramics. The hardening of the Poisson ratio is more pronounced in the Na-bearing term, but the change is minimal.

Unfortunately this treatment is missing from a recent study of the elasticity of $KAlSi_3O_8$ hollandite, which is based on the finite-differences approach (Mookherjee and Steinle-Neumann, 2009). Ignoring the rotation of the tensor induces differences in the shear bulk moduli in the Reuss formulation. These errors decrease the value of the Reuss shear modulus; their effect scales with the size of the $C_{16}$ elastic constants. As the value of the off-diagonal $C_{16}$ constants increases under compression, the errors induced by neglecting this term in the moduli formulation are more important in the high-pressure region.

The most remarkable feature of hollandite under pressure is the ferroelastic transition. This transition is seen in the first-principles calculations by the softening of the tetragonal shear, the $C_{11}$-$C_{12}$ combination of the elastic constants

in the Laue II setting and by the softening of the $C_{66}$ elastic constant in the Laue I setting. Apart form the softening of $C_{11}$-$C_{12}$, Mookherjee and Steinle-Neumann (2009) see softening of $C_{66}$ but also of $C_{11}$ in the Laue I setting. They both appear at larger pressures (more than 10%) than both the experimental measurements and our calculations for the ferroelastic transition. This discrepancy might be due to the use of supercells, as our calculations that use the alchemical approach yield a transition pressure within 2% of the experimental value.

For the K-pure phase $C_{66}$ becomes negative at about 23 GPa; for the Na-bearing composition the softening is faster, $C_{66}$ passing the elastic stability condition at about 13-14 GPa. This softening of $C_{66}$ is reflected in the softening of the Reuss elastic moduli that precedes the ferroelastic transition. For the K-end member both Y and G become negative at respectively 22 and 23 GPa. For the Na-bearing term both Y and G become negative at about 13-14 GPa (Figure 3). The theoretical instability values are slightly different than the experimental values of the phase transition, which are about 20 GPa for the K-pure term (Sueda et al. 2004; Nishiyama et al. 2005; Ferroir et al. 2006; Hirao et al. 2008) and about 17 GPa for the 20 %Na composition (Boffa Ballaran et al., 2009), but nevertheless remain within reasonable values expected within the density-functional theory. Moreover the coupling between the $B_g$ phonon mode that softens under pressure (Boffa Ballaran et al., 2009) and the shear instability may lead to a further adjustment of the theoretical transition pressure.

The variation of the compressional, $V_p$ and shear, $V_s$, seismic wave velocities for homogeneous aggregates as a function of pressure, as calculated from the Voigt elastic moduli, is represented in Figure 4. Both compositions show an increase of the wave velocities as a function of pressure. The Na-bearing term is slightly softer than the K-pure term. The difference goes from 0.2 % at a pressure of 0 GPa up to 1.7-1.8 % at pressures of 20 GPa for both $V_p$ and $V_s$, and up to 3.1 % for $V_p$ and to 4.3 % for $V_s$ at 40GPa. The density variation between the two compositions is mainly due to the difference in mass (2.55 %) and not so much to a difference in the volume of the unit cell (1.3 % at 40 GPa). However shear seismic waves traveling perpendicular to the tetragonal four-fold axis exhibit a strong decrease in velocity close to the ferroelastic transitions, as expected. This is obvious from Table 5 where we list the velocities of the seismic waves traveling along the [001] and the [100] directions.

The seismic anisotropy of the compressional waves decreases with increasing pressure and increases with Na content, but remains relatively weak. The seismic anisotropy of the shear waves, defined as the relative difference between the two shear components $(V_{s1}\text{-}V_{s2})/V_{s2}$, is instead very pronounced. This can be easily explained considering the crystal structure: the propagation of

the shear wave implies deformations of the framework of Al/SiO6 octahedra. These deformations are easily accommodated in the basal plane because of the weak K-O bonds and the square tunnels would deform to become rhombi. However the deformations of the octahedral framework along the fourfold axes involves octahedral tilts that require larger amounts of energy because of the edge-sharing connectivity and are unfavorable.

Despite being a minor phase, its shear wave anisotropy prior to the ferroelastic transition is strong enough for hollandite to be able to present a significant contribution to the mantle seismic anisotropy. The sedimentary cover of the subducting slabs is rich in K-bearing phases such as micas and feldspars. At moderate conditions, beyond the stability field of phengite micas, the only remaining K-bearing phase is hollandite. This will then be a common minor phase in subducting environments able to survive throughout the subduction cycle even down to the bottom of the lower mantle. Consequently any exhaustive study of the elastic and thermodynamic properties of the subducted sediments in the mantle need to take into account hollandite in order to be complete.

Even if it would not be seismically visible by itself, the presence of hollandite in subducting slabs would release some of the constraints that are imposed on the lattice-preferred orientation of olivine and pyroxene crystals (Mainprice et al., 2000, Karato et al., 2008) to explain the seismic observations. Thus our results show that further mineralogical and seismic models of K-rich regions of the upper mantle should also consider the seismic signature of hollandite and of its ferroelastic transition.

## 4 Acknowledgments

This research was supported by the Alexander von Humboldt foundation. The calculations were performed on the jade machine at CINES under x20080825134 computational grant.

## References

[1] Akaogi, M., Kamii, N., Kishi, A., Kojitani, H., 2004, Calorimetric study on high-pressure transitions in $KAlSi_3O_8$. Phys. Chem. Minerals, 31, 85-91.

[2] Baroni, S., Giannozzi, P., Testa, A., 1987. Greens-function approach to linear response in solids, Phys. Rev. Lett., 58, 1861-1864.

[3] Baroni, S., de Gironcoli, S., Dal Corso, A., Giannozzi, P., 2001. Phonons and related crystal properties from density-functional perturbation theory, Rev. Mod. Phys., 73, 515-562.

[4] Bellaiche, L., and Vanderbilt, D., 2000. Virtual crystal approximation revisited: Application to dielectric and piezoelectric properties of perovskites, Phys. Rev. B 61, 7877-7882.

[5] Blanchfield, P., Saunders, G.A., and Hailing, T., 1982, The hydrostatic pressures derivatives of the elastic constants of the scheelites $LiYF_3$ and $LiY_{0.5}Tb_{0.5}F_4$, J. Phys. C.: Solid State Phys., 15, 2081-2092.

[6] Boffa Ballaran, T., Liu, J., Dubrovinsky, L.S., Caracas, R. and Crichton, W., 2009, High-pressure ferroelastic phase transition in aluminosilicate hollandite, Phys. Rev. B 80, 214104.

[7] Caracas, R., 2002, A database of incommensurate phases. J. Appl. Cryst. 35, 120-121.

[8] Caracas, R., E.J. Banigan, 2009, Elasticity and Raman spectra of MgAl2O4 spinel from density functional perturbation theory, Phys. Earth Planet. Inter., 174, 113-121.

[9] Cohen, M.L., 2007, *Quantum alchemy* in Chemistry for the 21st century, Eds. E. Keinan and I. Schechter. Wiley-VCH.

[10] Dobrzhinetskaya, L.F., and Green, H.W., 2007, Experimental studies of mineralogical assemblages of metasedimentary rocks at Earth's mantle transition zone conditions, J. Metamophic Geol., 25, 83-96.

[11] Downs, R.T., Hazen, R.M., and Finger L.W., 1995, Crystal chemistry of lead aluminosilicate hollandite: A new high-pressure synthetic phase with octhaedral Si, Amer. Mineral., 80, 937-940.

[12] Farley, J.M., Saunders, G.A., and Chung, D.Y., 1975. Elastic properties of scheelite structure molybdats and tungstates, J. Phys. C.: Solid State Phys., 8, 780-786.

[13] Ferroir, T., Onozawa, T., Yagi, T., Merkel, S., Miyajima, N., Nishiyama, N., Irifune, T., and Kikegawa, T., 2006. Equation of state and phase transition in $KAlSiO_3O_8$ hollandite at high pressure, Amer. Mineral., 91, 327-332.

[14] Giantomassi, M., Boeri, L., and Bachelet, G.B., 2005. Electrons and phonons in the ternary alloy $CaAl_{2-x}Si_x$ as a function of composition, Phys. Rev. B, 72, 224512.

[15] Gonze, X., Allan, D.C., Teter, M.P., 1992. Dielectric tensor, effective charges and phonon in a-quartz by variational density-functional perturbation theory, Phys. Rev. Lett., 68, 3603-3606.

[16] Gonze, X., 1997. First-principle responses of solids to atomic displacements and homogeneous electric fields: Implementation of a conjugate-gradient algorithm, Phys. Rev. B, 55, 10337-10354.

[17] Gonze, X., Lee, C., 1997. Dynamical matrices, born effective charges, dielectric permittivity tensors, and interatomic force constants from density-functional perturbation theory, Phys. Rev. B, 55, 10355-10368.

[18] Gonze, X., J.M. Beuken, R. Caracas, F. Detraux, M. Fuchs, G.M. Rignanese, L. Sindic, M. Verstraete, G. Zerah, F. Jollet, M. Torrent, A. Roy, M. MIkami, Ph. Ghosez, J.Y. Raty, D.C. Allan, 2002. First-principles computation of material properties: the ABINIT software project. Computational Materials Science, 25, 478-492.

[19] Gonze, X., G.M. Rignanese, M. Verstraete, J.M. Beuken, Y. Pouillon, R. Caracas, F. Jollet, M. Torrent, G. Zerah, M. Mikami, P. Ghosez, M. Veithen, V. Olevano, L. Reining, R. Godby, G. Onida, D. Hamann, and D.C. Allan, 2005. A brief introduction to the ABINIT software package. Zeitschrift für Kristallographie, 220, 558.

[20] Gonze, X., Rignanese, G.-M., Caracas, R., 2005a. First-principles studies of the lattice dynamics of crystals, and related properties, Z. Kristallogr., 220, 458-472.

[21] Hamann, D., Wu, X., Rabe, K.M. and Vanderbilt D., 2005. Metric tensor formulation of strain in density-functional perturbation theory, Phys. Rev. B 71, 035117.

[22] Hirao, N., Ohtani, E., Kondo, T., Sakai, T. and Kikegawa, T., 2008. Hollandite II phase in $KAlSi_3O_8$ as a potential host mineral of potassium in the Earth's lower mantle, Phys. Earth Planet. Inter., 166, 97-104.

[23] Hohenberg, P., and W. Kohn. 1964. Inhomogenous electron gas. Physical Review, 136, 864B-871B.

[24] Irifune, T., Ringwood, A.E., and Hibberson, W.O., 1994, Subduction of continental crust and terrigenous and pelagic sediments: an experimental study. Earth Planet. Sci. Lett., 126, 351-368.

[25] Karato, S.-I., Jung, H., Katayama, I., and Skemmer, P., 2008. Geodynamic significance of seismic anisotropy of the upper mantle: new insights from laboratory studies. Annu. REv. Earth Planet. Sci., 36, 59-95.

[26] Kohn, W., and L.J. Sham, 1965. Self-consistent equations including exchange and correlation effects. Physical Review, 140, 1133A-1138A.

[27] Konzett, J., and Fei, Y., 2000, Transport and storage of potassium in the Earth's upper mantle and transition zone: an experimental study to 23 GPa in simplified and natural bulk compositions. J. Petrol., 41, 583-603.

[28] Liu, X., 2006, Phase relations in the system $KAlSi_3O_8$-$NaAlSi_3O_8$ at high pressure - high temperature conditions and thier implications for the petrogenesis of lungunite. Earth Planet. Sci. Lett., 246, 317-325.

[29] Mainprice, D., Barroul, G., and Ben Ismail, W., 2000. The seismic anisotropy of the Earth's mantle: from single crystl to polycrystal. In *Earth's Deep Interior*, eds. Karato, S.-I., Forte, A., Liebermann, R.C., Masters, G., and Stixrude, L., 237-64, Washington, DC. AGU.

[30] Monkhorst, H.J., Pack, J.D., 1976. Special points for Brillouin-zone integrations, Phys. Rev. B, 13, 5188- 5192.

[31] Mookherjee, and G. Steinle-Neumann, 2009. Detecting deeply subducted crust from the elasticity of hollandite, Earth Planet. Sci. Lett., 288, 349-358.

[32] Nishiyama, N., Rapp, R.P., Irifune, T., Sanehira, T., Yamazaki, D., and Funakoshi, K., 2005, Stability and P-V-T equation of state of $KAlSi_3O_8$-hollandite determined by in situ X-ray observations and implications for dyhnamics of subducted continenetal crust material, Phys. Chem. Minerals, 32, 627-637.

[33] Payne, M.C., M.P. Teter, D.C. Allan, T.A. Arias, and J.D. Joannopoulos, 1992. Iterative minimization techniques for ab initio total-energy calculations: molecular dynamics and conjugate gradients. Reviews in Modern Physics, 64, 1045-1097.

[34] Schmidt, M.W., 1996. Experimental constraints on recylcing of potassium from subducted oceanic crust. Science, 272, 1927-1930.

[35] Sueda, Y., T. Irifune, N. Nishiyama, R. P. Rapp, T. Ferroir, T. Onozawa, T. Yagi, S. Merkel, N. Miyajima, and K. Funakoshi, 2004. A new high-pressure form of $KAlSi_3O_8$ under lower mantle conditions, Geophys. Res. Lett., 31, L23612, doi:10.1029/2004GL021156.

[36] Tutti, F., Dubrovinsky, L.S., Saxena, S.K., and Carlson, S., 2001, Stability of $KAlSi_3O_8$ hollandite-type structure in the Earth's lower mantle conditions, 28, 2735-2738.

[37] Urakawa, S., Kondo, T., Igawa, N., Shimomura, O., and Ohno, H., 1994, Synchrotron radiation study on the high-pressure and high-temperature phase relations of $KAlSi_3O_8$, 21, 387-391.

[38] Wu, X.-J., Fujiki, Y., Ishigame, M., and Horiuchi, S., 1991, Modulation mechanism and disorder structure in hollandite-type crystals, Acta Cryst., A476, 405-413.

[39] Yagi, A., Suzuki, T., and Akaogi, M., 1994, High-pressure transitions in the system $KAlSi_3O_8$-$NaAlSi_3O_8$. Phys. Chem. Minerals, 21, 12-17.

[40] Yong, W., Dachs, E., Withers, A.C., and Essene, E.J., 2006, Heat capacity and phase equilibria of hollandite polymorph of $KAlSi_3O_8$. Phys. Chem. Minerals, doi: 10.1007/s00269-006-0063-4.

Table 1
Variation of the lattice parameters with pressure for $KAlSi_3O_8$ (columns 2-4) and $K_{0.8}Na_{0.2}AlSi_3O_8$ (columns 5-7) hollandite. Values correspond for the conventional unit cell. The structural anisotropy, defined as a/c is remarkably unaffected by chemistry.

| P(GPa) | a (Å) | c(Å) | a:c | a(Å) | c(Å) | a:c |
|---|---|---|---|---|---|---|
| 0 | 9.203 | 2.694 | 3.416 | 9.157 | 2.683 | 3.413 |
| 5 | | | | 9.078 | 2.668 | 3.403 |
| 10 | | | | 9.007 | 2.654 | 3.394 |
| 20 | 8.928 | 2.642 | 3.380 | 8.885 | 2.629 | 3.379 |
| 40 | 8.725 | 2.600 | 3.356 | 8.687 | 2.587 | 3.358 |

Table 2
Variation of the reduced general atomic coordinates of hollandite. There is a weak dependence with pressure due to the rigidity of the tetragonal tunnels. The xT and yT are respectively the x and y coordinates of the cations residing in the tetrahedral sites. the other columns relates to the oxygen coordinates.

| P(GPa) | xT | yT | xO1 | yO1 | xO2 | yO2 |
|---|---|---|---|---|---|---|
| $KAlSi_3O_8$ | | | | | | |
| 0 | 0.350 | 0.166 | 0.154 | 0.203 | 0.541 | 0.164 |
| 20 | 0.350 | 0.167 | 0.152 | 0.199 | 0.541 | 0.164 |
| 40 | 0.350 | 0.168 | 0.151 | 0.196 | 0.542 | 0.164 |
| $K_{0.2}Na_{0.2}AlSi_3O_8$ | | | | | | |
| 0 | 0.351 | 0.167 | 0.153 | 0.201 | 0.542 | 0.164 |
| 5 | 0.351 | 0.167 | 0.153 | 0.200 | 0.542 | 0.164 |
| 10 | 0.351 | 0.167 | 0.152 | 0.199 | 0.542 | 0.164 |
| 20 | 0.351 | 0.168 | 0.151 | 0.197 | 0.542 | 0.164 |
| 40 | 0.351 | 0.169 | 0.150 | 0.194 | 0.542 | 0.164 |

Table 3
Elastic constants (in GPa) computed using the density functional perturbation theory for $KAlSi_3O_8$ and $K_{0.8}Na_{0.2}AlSi_3O_8$ hollandite as a function of pressure (P, in GPa). MSN = values taken from Mookerjeee and Steinle-Neumann, 2009.

| P | $C_{11}$ | $C_{33}$ | $C_{12}$ | $C_{13}$ | $C_{44}$ | $C_{66}$ | $C_{16}$ | $C_{11}$-$C_{12}$ |
|---|---|---|---|---|---|---|---|---|
| $K_1Na_0$ | | | | | | | | |
| 0 | 303 | 517 | 202 | 123 | 175 | 139 | 44 | 101 |
| 20 | 403 | 651 | 310 | 150 | 189 | 189 | 75 | 93 |
| 40 | 502 | 780 | 453 | 225 | 243 | 174 | 115 | 49 |
| 0[MSN] | 342 | 568 | 186 | 118 | 165 | 129 | - | |
| $K_{0.8}Na_{0.2}$ | | | | | | | | |
| 0 | 303 | 556 | 187 | 111 | 167 | 116 | 46 | 116 |
| 5 | 298 | 581 | 207 | 121 | 174 | 110 | 55 | 91 |
| 10 | 322 | 600 | 236 | 132 | 182 | 113 | 63 | 85 |
| 20 | 342 | 648 | 288 | 145 | 188 | 124 | 72 | 55 |

Table 4
Voigt-averaged elastic bulk (K), shear (G) and Young (Y) moduli (in GPa), Poisson's ratio ($\nu$), density ($\rho$, in g/cm$_3$) and the corresponding compressional ($V_p$) and shear ($V_s$) wave velocities (in km/s) for $KAlSi_3O_8$ and $K_{0.8}Na_{0.2}AlSi_3O_8$ hollandite as a function of pressure (P, in GPa). MSN = values taken from Mookerjeee and Steinle-Neumann, 2009.

| P | K | G | Y | $\nu$ | $\rho$ | $V_p$ | $V_s$ |
|---|---|---|---|---|---|---|---|
| $K_1Na_0$ | | | | | | | |
| 0 | 224 | 143 | 353 | 0.237 | 3.993 | 10.19 | 5.98 |
| 20 | 297 | 170 | 428 | 0.260 | 4.327 | 11.00 | 6.26 |
| 40 | 399 | 191 | 494 | 0.294 | 4.604 | 11.91 | 6.44 |
| 0[MSN] | 234 | 145 | 361 | 0.245 | | | |
| $K_{0.8}Na_{0.2}$ | | | | | | | |
| 0 | 220 | 140 | 347 | 0.237 | 3.938 | 10.17 | 5.97 |
| 5 | 231 | 140 | 350 | 0.247 | 4.029 | 10.18 | 5.90 |
| 10 | 249 | 145 | 364 | 0.257 | 4.113 | 10.37 | 5.93 |
| 20 | 276 | 150 | 382 | 0.270 | 4.177 | 10.68 | 6.00 |

Table 5
Seismic wave velocities (in km/s) as a function of direction of wave propagation in $KAlSi_3O_8$ (columns 2-3) and $K_{0.8}Na_{0.2}AlSi_3O_8$ hollandite (columns 4-6) vs. pressure (in GPa). The azimuthal seismic anisotropies, defined here as (Vmax-Vmin)/Vmin and expressed in % are listed in the last two columns. The values absent correspond to the onset of the shear instability.

| P | $V_p$ | $V_s$ | $V_p$ | $V_{s1}$ | $V_{s2}$ | An. $V_p$ | An. $V_s$ |
|---|---|---|---|---|---|---|---|
| $\parallel$ 001 | | | | | | | |
| 0 | 11.38 | 6.62 | 10.12 | 6.62 | 2.83 | 11.1 | 57.2 |
| 20 | 12.27 | 6.61 | 11.20 | 6.61 | 1.18 | 8.7 | 82.2 |
| 40 | 13.02 | 7.26 | 12.44 | 7.26 | | 4.4 | |
| $\parallel$ 100 | | | | | | | |
| 0 | 11.88 | 6.51 | 9.90 | 6.51 | 2.85 | 16.7 | 56.2 |
| 5 | 12.01 | 6.57 | 9.89 | 6.57 | 1.80 | 17.7 | 72.7 |
| 10 | 12.08 | 6.65 | 10.21 | 6.65 | 1.10 | 15.4 | 83.4 |
| 20 | 12.46 | 6.71 | 10.69 | 6.71 | | 14.2 | |
| 40 | 12.87 | 7.29 | 11.95 | 7.29 | | 7.1 | |

Fig. 1. Crystal structure of hollandite viewed along the fourfold axis.

Fig. 2. Pressure dependence of the elastic constants of the tetragonal structure of $KAlSi_3O_8$ (upper panel) and $K_{0.8}Na_{0.2}AlSi_3O_8$ (lower panel) hollandite in the Laue TI setting. In this setting all elastic constants harden with pressure, except for the pure shear $C_{66}$ constant that softens and become negative at the ferroelastic transition pressure. The effect of the K-Na substitution with up to 20% Na is minimal all the constants, the only clear change being the more rapid softening of $C_{66}$ in case of the Na-bearing composition.

Fig. 3. Pressure dependence of the bulk (K), shear (G) and Young (Y) elastic moduli of the tetragonal structure of $KAlSi_3O_8$ and $K_{0.8}Na_{0.2}AlSi_3O_8$ hollandite in the Voigt and Reuss formulations. The Voigt averaged moduli show an increase with pressure. The Reuss averaged moduli are more sensitive to the elastic softening and mark the ferroelastic phase transition occurring under pressure. The phase transition pressure is lowered from about 25GPa for the K-pure term to 13 GPa for Na-bearing composition.

Fig. 4. Pressure dependence of the seismic wave velocities of $KAlSi_3O_8$ and $K_{0.2}Na_{0.8}AlSi_3O_8$ in the Voigt formulation. Na softens hollandite for both $V_p$ and $V_s$. The change in density follows the same pattern but is less evident than for $V_p$ and $V_s$.

**Figure 1**

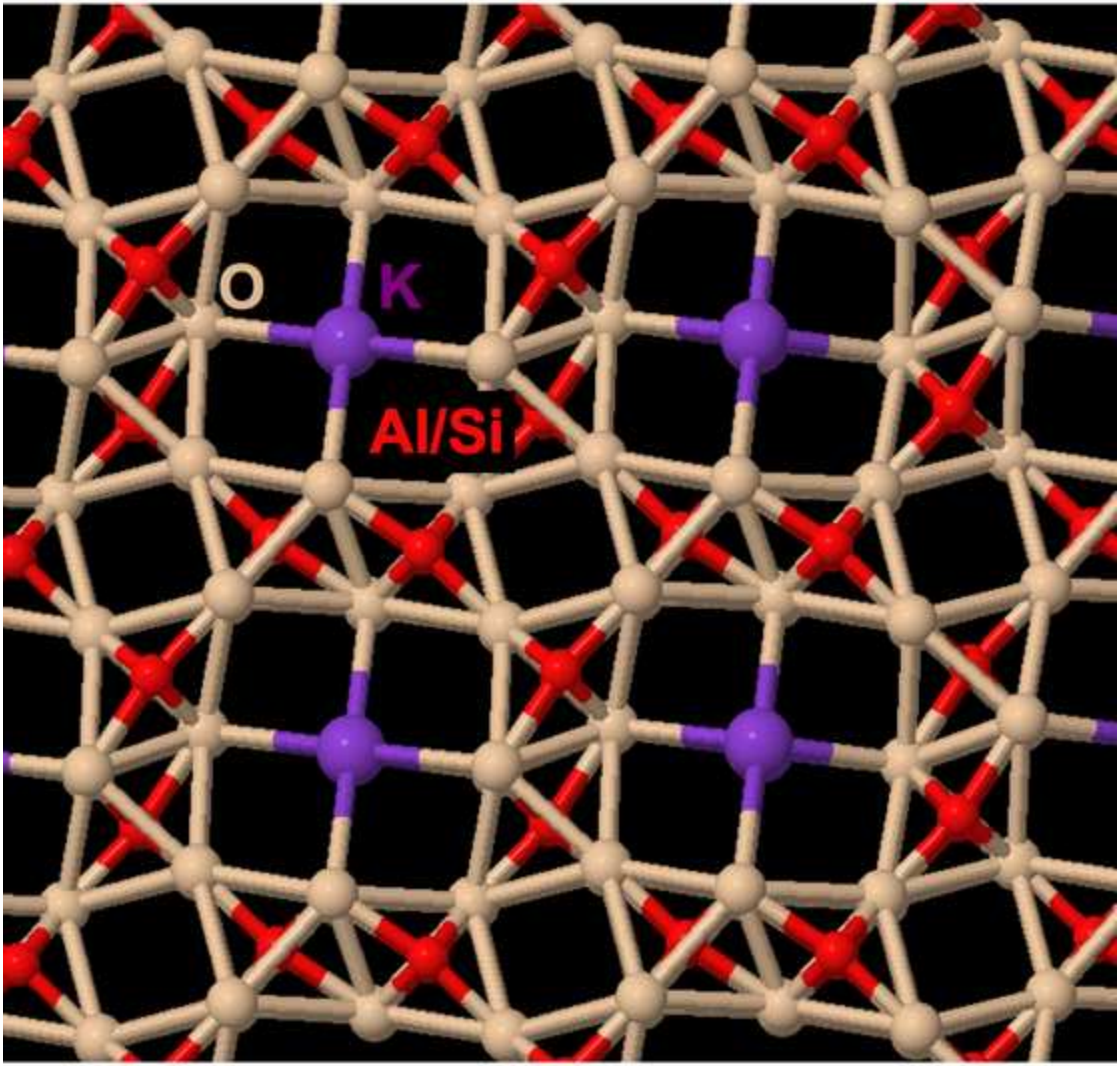

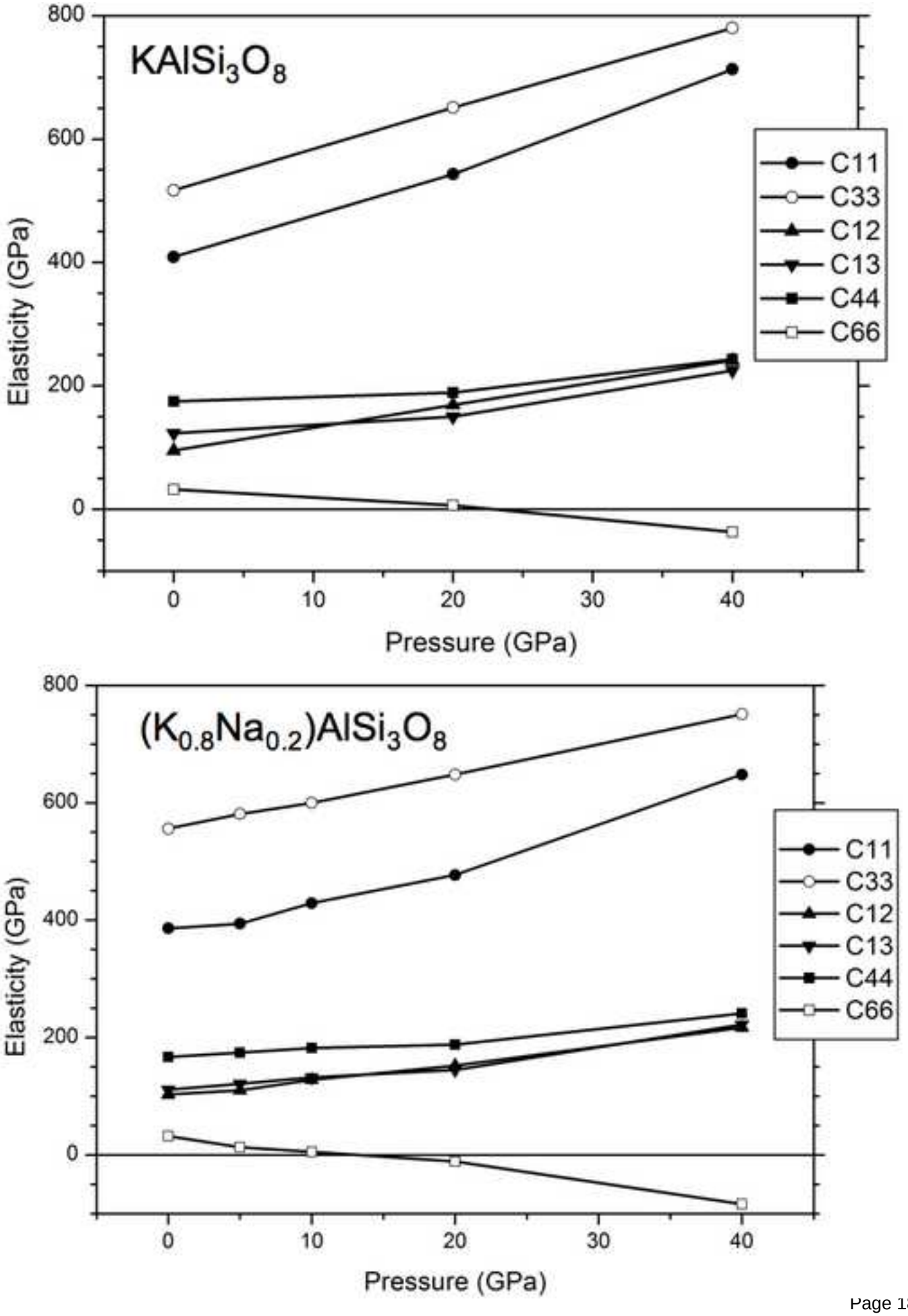

**Figure 3**

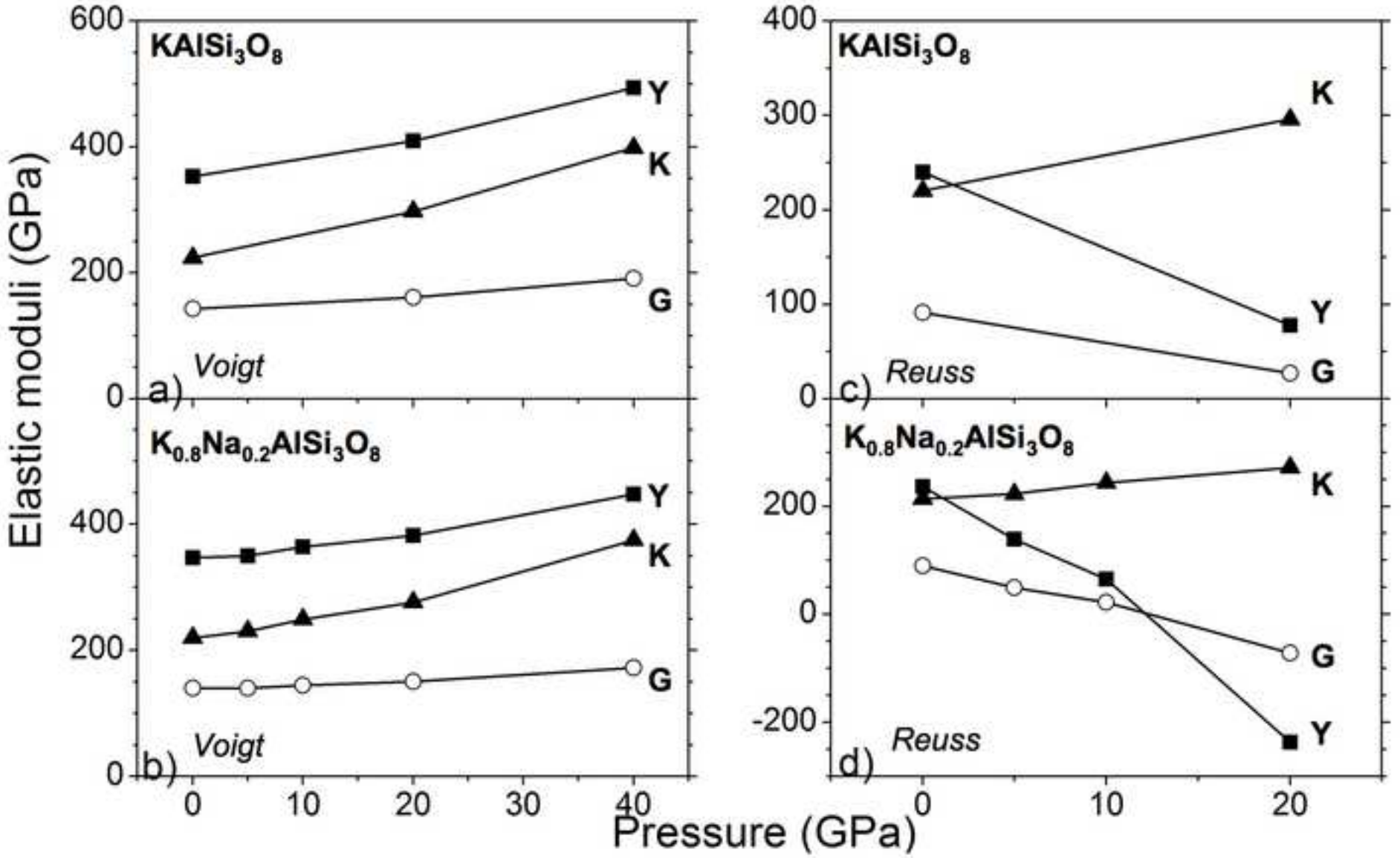
KAlSi3O8
K0.8Na0.2AlSi3O8
Y
K
G
Voigt
Reuss
a)
b)
c)
d)
Elastic moduli (GPa)
Pressure (GPa)
600
400
200
0
300
100
-200
10
20
30
40

**Figure 4**

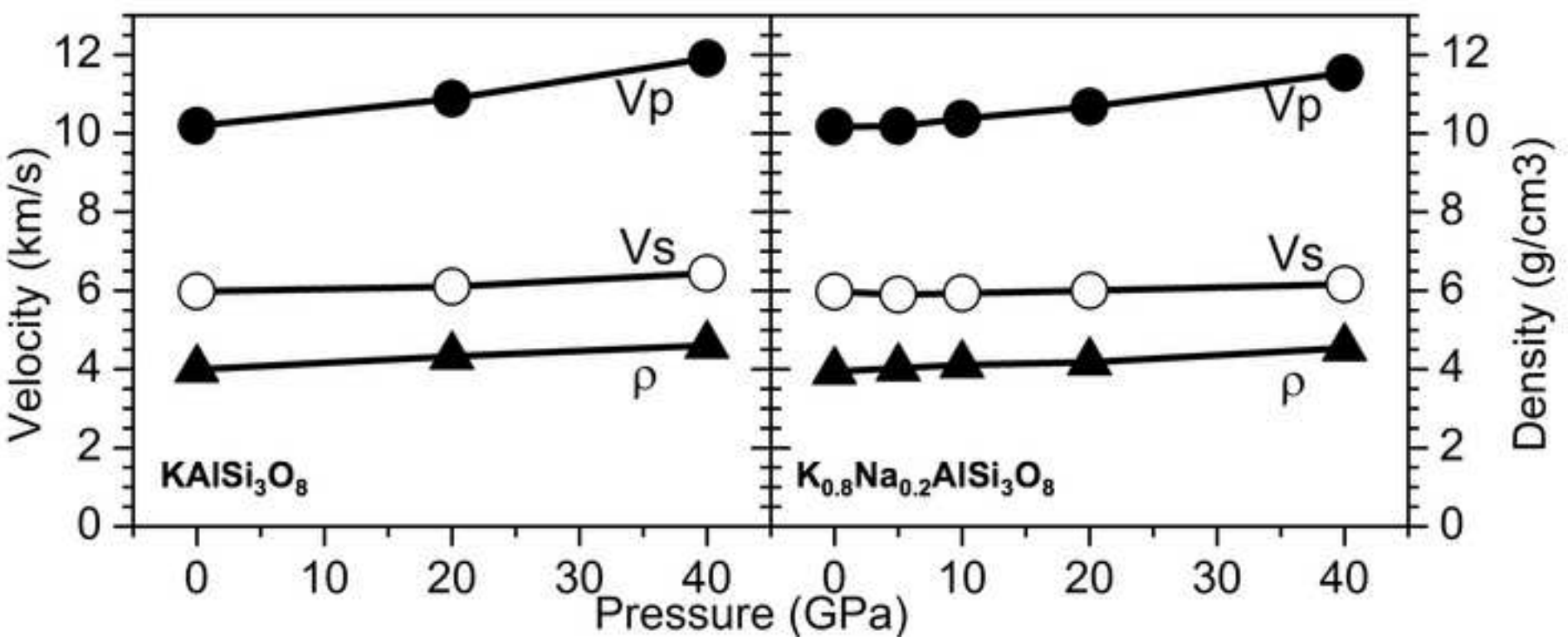
Velocity (km/s)
Density (g/cm3)
Pressure (GPa)
Vp
Vs
ρ
KAlSi3O8
K0.8Na0.2AlSi3O8
0
2
4
6
8
10
12
0
10
20
30
40